The AGN-galaxy connection: Low-redshift benchmark & lessons learnt

Stéphanie Juneau[iD]

National Optical Astronomy Observatory, Tucson AZ 85719, USA
email: sjuneau@noao.edu

Abstract. Several scenarios have been proposed to describe the physical connection between galaxies and their central active galactic nuclei (AGN). This connection could act on a range of spatial scales and vary across cosmic time. In these proceedings, we consider black hole and galaxy growth and whether that growth is affected by AGN feedback both based on statistical approaches − which reveal general population trends − and based on an individual case study − which gives us a more detailed insight on the physical processes at play. For the statistical approach, we showcase a low-redshift $(0.04 < z < 0.2)$ SDSS sample with AGN classification based on a combination of emission-line diagnostic diagrams, and for which we account for sample selection by using a V/V_{max} approach. The trends on the star formation rate - stellar mass $(SFR - M_\star)$ plane suggest that the most likely connection is a common gas reservoir for star formation and AGN, and that they both decline as the gas reservoir is consumed. The trends established at low-redshift could act as a local benchmark against which to compare higher redshift studies. As a complementary approach, we use a detailed case study of a nearby AGN host with integral field spectroscopy from the VLT/MUSE instrument in order to spatially resolve the interplay between AGN feedback and the host galaxy. We find that the galaxy substructure likely plays a role by collimating and/or obscuring the outflows and radiation from the central engine. Ongoing and future work with 3D spectroscopy will enable us to learn more about galaxy and black hole coevolution. Lastly, we briefly discuss lessons learnt from both approaches.

Keywords. galaxies: active, galaxies: fundamental parameters (classification), galaxies: Seyfert, galaxies: evolution, galaxies: individual (NGC 7582)

1. Introduction: AGN fueling & feedback

The growth of galaxies and that of their supermassive black holes (SMBHs) may be physically connected given the observed scaling relations between them (e.g., Magorrian *et al.* 1998; Ferrarese & Merritt 2000, but also see Jahnke & Maccío 2011). Therefore one can ask whether the mechanism responsible for the BH growth itself (AGN fueling) is related to host galaxies properties, and vice versa. Alternatively, it could be that the culprit is a mechanism regulating or stopping the growth of BHs and galaxies, such as AGN feedback. Cosmological simulations need a source of energy to regulate and suppress star formation in galaxies in order to reproduce the observed galaxy distribution functions (e.g., Bower *et al.* 2006; Gabor & Davé 2012; Hirschmann *et al.* 2014), which is often attributed to AGN feedback (e.g., Croton *et al.* 2006; Schaye *et al.* 2015). The flavors of feedback include a maintenance (or radio) mode according to which AGN inject mechanical energy into their surrounding medium, keep it too hot to form stars (e.g., Ciotti *et al.* 2010; Karouzos *et al.* 2014), and a radiative (or quasar) mode that is postulated to expel material in the form of outflows which likely originate as accretion disk winds (e.g., Beckmann *et al.* 2017; Harrison *et al.* 2018; also see reviews by Fabian 2012 and Harrison 2017).

In order to learn about the processes driving AGN fueling and AGN feedback, one can consider AGN activity as a function of host galaxy properties. So far, different results have been obtained for various galaxy and/or AGN selection methods, which emphasizes the need to understand sample selection. For example, some studies found that AGN were predominantly hosted in star forming galaxies (e.g., Silverman *et al.* 2009; Rosario *et al.* 2013), while others found that their host galaxies had on average lower star formation rates (SFRs) compared to normally star-forming galaxies (e.g., Mullaney *et al.* (2015)) and that they tend to occupy the transition region between star-forming and passive galaxies in terms of their colors and/or SFRs (e.g., Schawinski *et al.* 2007). Yet other studies reported that galaxies' stellar mass may be a better determinant of AGN fueling than SFRs (e.g., Bongiorno *et al.* 2012; Tanaka 2012). Furthermore, there are disagreements about the role of galaxy mergers in affecting (or not) the presence and feedback from AGN (e.g., Kartaltepe *et al.* 2010; Treister *et al.* 2012; Grogin *et al.* 2005; Cisternas *et al.* 2011; Steinborn *et al.* 2018). Different AGN selection methods based on various wavebands (optical, infrared, radio, X-rays, etc.) can also lead to different results (e.g., Hickox *et al.* 2009; Juneau *et al.* 2013; Ellison *et al.* 2016).

In these proceedings, we revisit the situation at low redshift with a well-defined selection function in order to establish a reference benchmark to compare with other work. We first consider a statistical approach by looking at the galaxy evolution context as quantified by the location of galaxies on the star formation rate (SFR) - stellar mass ($M_\star$) plane (Section 2). We then move on to the detailed case study where we investigate the gas ionization properties and the kinematics of the stars and gas in order to paint a picture of AGN feedback in relation to the host galaxy substructure (Section 3). We conclude each section with lessons learnt and a few open questions that motivate future effort.

2. AGN fueling & feedback: Low-Redshift Benchmark

The first part of these proceedings consists of a statistical approach in order to identify global trends of AGN fueling and feedback. Given that AGN variability can occur on much shorter timescales relative to galaxies' dynamical time, averaging large ensembles can give us an overview of the overall trends (e.g., Chen *et al.* 2013).

2.1. *Sample Selection*

Motivated by the need to revisit a low-redshift benchmark to understand the AGN-galaxy connection, we selected a sample based on the Sloan Digital Sky Survey survey (SDSS) DR7 (Abazajian *et al.* 2009). We opted to use SDSS-II rather than SDSS-III because the main galaxy sample is more uniformly selected with magnitude limits of $14.5 < r < 17.77$, which helps to compute volume correction factors to account for selection effects. Because we are interested in understanding the host galaxy properties, the bulk of the analysis concerns Type 2 AGNs, for which the nuclear light is optically obscured, therefore giving us access to spectral and photometric diagnostics of the host galaxy stellar content. A complete account of AGN including Type 1 is estimated by applying a correction factor for the Type 1/Type 2 ratio, which is observed to depend on AGN luminosity (e.g., Simpson 2005; Lusso *et al.* 2013), and assuming that this ratio does not otherwise vary strongly as a function of SFR and $M_\star$.

The sample selection was done similarly to the study by Juneau *et al.* (2014, hereafter J14) by requiring the signal-to-noise ratio of the emission line ratios [O III]/Hβ and [N II]/Hα to be above $3/\sqrt{2}$ ($\approx$2.12), after applying the corrections to the reported Hβ fluxes for Balmer absorption correction (Groves *et al.* 2012), and after applying the emission line ratio uncertainty scalings that J14 determined from comparing duplicate

observations (their Appendix A). These emission line ratios are used to classify the ionization source of the galaxies as described in the *Method* below. We further applied a redshift cut of $0.04 < z < 0.2$, and required an available value of stellar mass ($\log(M_\star/M_\odot) > 6$). We used the MPA-JHU Value-Added Catalogs (VACs)† generated following the methods described by Kauffmann *et al.* (2003a), Brinchmann *et al.* (2004), and Tremonti *et al.* (2004).

2.2. *Method*

Starting from the observed and derived properties from the SDSS dataset and associated VACs as described above, we need to identify the presence of AGN, derive additional properties such as the AGN bolometric luminosity (L_{bol}), and to compute correction factors to account for selection effects in order to obtain an overall census of the galaxy populations. We describe these steps below.

AGN Classification. We identify the presence of AGN in galaxies according to emission line diagnostic diagrams. Namely, we use their locus on the BPT (Baldwin *et al.* 1981) and VO87 (Veilleux & Osterbrock 1987) diagrams. These diagnostic diagrams consist of [O III]/Hβ as a function of, respectively, [N II]/Hα, and [S II]/Hα. On the BPT, we use the demarcation line determined by Kauffmann *et al.* (2003b) in order to distinguish between star-forming galaxies (lower left) and the rest. The higher demarcation from Kewley *et al.* (2001) further distinguishes between AGN (above and to the right), and composite galaxies which are located between the two demarcations. The VO87 diagram is more sensitive to shock and/or post-AGB ionization, and therefore can more readily separate Seyfert-like ionization from LINER-like ionization. We used the demarcations from Kewley *et al.* (2006) in this case. Below, we consider the galaxy population separated according to AGN bolometric luminosities.

AGN Bolometric Luminosity. Low-redshift, massive galaxies tend to be metal-rich (e.g., Tremonti *et al.* 2004). As a result, their [O III] emission lines are dominated by AGN activity when present ($\sim$93% AGN contribution; Kauffmann *et al.* 2003b). We use the [O III] luminosity as a proxy, and apply a bolometric correction factor to estimate the AGN bolometric luminosites. We correct the emission line for foreground dust attenuation following Bassani *et al.* (1999) and assuming an intrinsic Balmer Decrement Hα/Hβ value of 3.0 appropriate for NLR gas (Osterbrock & Ferland 2006). We then employ the Lamastra *et al.* (2009) bolometric correction factor

Type 1 AGN Correction. Type 1 AGN were not explicitly included in our sample due to additional uncertainties in accessing the host stellar properties in the presence of a point source. The brightest type 1 AGNs (quasars) were also targeted separately from the selection function of the SDSS *main* galaxy sample. However, we estimate their contribution to the total number (and fraction) of AGN based on the assumption that they share similar host galaxies as Type 2 AGNs, and that their contribution can be derived from the obscured (Type 2) fraction. Following the work by Lusso *et al.* (2013), we adopt the functional form of a modified receding torus model proposed by Simpson 2005, which predicts the following relationship between the obscured fraction f_{obsc} and AGN bolometric luminosity:

$$f_{obsc} = [1 + 3(L_{bol}/L_0)^{1-2\xi}]^{-0.5}, \qquad (2.1)$$

where we use the values found by Lusso *et al.* (2013) for their main sample (optically thin case) of $L_0 = 10^{46.16}$ erg s^{-1} and $\xi = 0.37$. We convert into statistical weights $w_{obsc} = 1/f_{obsc}$ to use when computing the number and fraction of AGN based on the obscured (Type 2) number and fraction. We note that the optically-thick case predicts

† http://www.mpa-garching.mpg.de/SDSS/DR7/
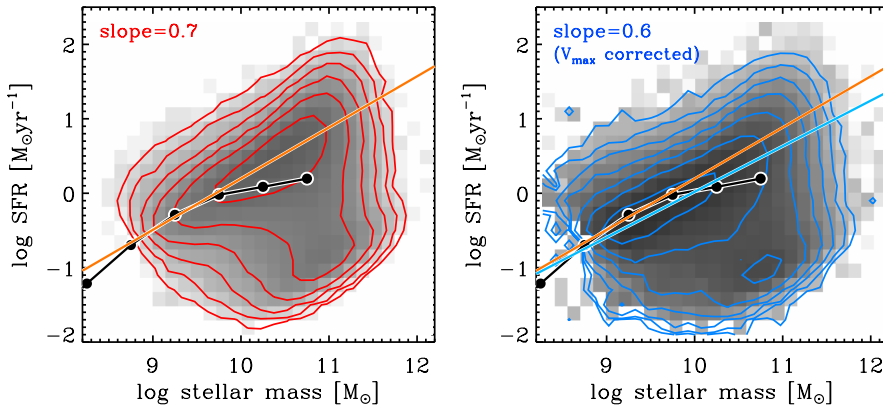
Figure 1. SFR-$M_\star$ plane for the SDSS $0.04 < z < 0.2$ galaxy sample. *Left.* Bivariate distribution of our sample before applying the V/V_{max} correction factors. The contours are logarithmically spaced by 0.5 dex. The best-fit linear relationship calculated for the non-AGN galaxies with $9.2 < \log(M_\star/M_\odot) < 10.7$ is shown with the orange line. The black circles show the low-mass sample of Gavazzi *et al.* (2015). *Right.* Same as the left-hand panel, except after applying the V/V_{max} correction factors. In addition to the current best-fit linear relation to the mode of the non-AGN galaxies (solid blue line), we overlay the best-fit relationship from the left-hand panel (solid orange line) for comparison. We find a slope that is flatter by 0.1 after correcting for the detection limits using the V/V_{max} technique.

lower obscured fractions, and consequently higher total number and fraction of AGN relative to what is reported here. However, our implementation of the statistical weights mostly affects the normalization of the bivariate distributions on the SFR-$M_\star$ plane, and not much the locus or shape of the contours (Section 2.3).

V/V_{max} *Correction.* In order to account for the selection functions of both the SDSS *main* galaxy sample, which is magnitude limited, and of the emission-line criterion, we define separately the maximum volume within which a given object would be detected (V_{max}) for both selection steps, and keep the minimum value as the most stringent limit. The photometric selection is $14.5 < r < 17.77$. For each galaxy in our sample, we compute the k-correction using the dereddened $ugriz$ photometry converted to AB magnitudes to predict the observed r band magnitude over a range of redshifts in order to determine z_{min} — the minimum redshift allowed before the object is too bright ($r < 14.5$) — and z_{max} — the maximum redshift before the object is too faint ($r > 17.77$). We store these values to compare with the maximum redshift at which the [O III]/Hβ and [N II]/Hα emission line ratios are still detected with $S/N > 3/\sqrt{2}$, which we define as z_{max}^{lines}, and we keep $z_{max} = min(z_{max}, z_{max}^{lines})$.

Lastly, we compute the maximum detectable co-moving volume element within — and normalized by — the co-moving volume from the redshift range of interest ($0.04 < z < 0.2$). The resulting V/V_{max} values are used as statistical weights when generating bivariate distributions such as the SFR-$M_\star$ plane, which will be the main parameter space to set our analysis within the galaxy evolution context. In Figure 1, we show the bivariate distribution of the full sample before and after applying the V/V_{max} correction factors. In both panels, there is a fairly tight sequence of star-forming galaxies with rising SFRs as a function of $M_\star$, and a population of passive (and/or quenched) galaxies with comparatively lower SFRs. Applying the V/V_{max} correction changes the relative proportions of galaxies within the parameter space. As expected, the correction is much more pronounced at the low-mass end (until the original sample runs out of galaxies altogether, which explains the sharp cutoff at the low SFR-$M_\star$ portion of the right-hand side panel). Also unsurprisingly, at a given stellar mass, the correction is more important
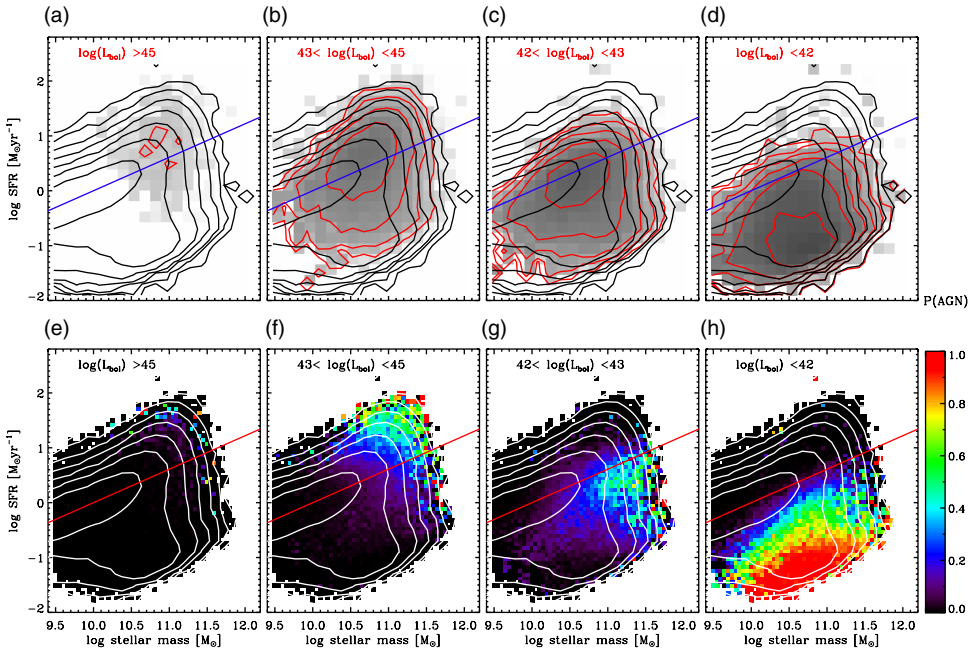
Figure 2. SFR-$M_\star$ plane for the SDSS $0.04 < z < 0.2$ galaxy sample. The top row shows the bivariate distribution of AGN in bins of bolometric luminosity as labeled (grey shaded and red contours), overlaid on the bivariate distribution of the full galaxy population (black contours), which is identical on all panels. The bottom row displays the same galaxy population except that in each panel, the SFR-$M_\star$ bins are color-coded by the fraction of galaxies hosting an AGN within the labeled AGN luminosity range (color bar). This AGN fraction could correspond to a duty cycle assuming that all galaxies in a given bin of SFR and $M_\star$ go through *on* and *off* phases.

for objects with a lower SFR. As a result, the sequence is slightly lower after correcting for V/V_{max}. A linear fit to the mode of the $\log(\text{SFR})$-$\log(M_\star)$ distribution for BPT-SF galaxies is shown before (orange) and after (blue) applying the correction. The final slope is slightly flatter at 0.6 relative to the value of 0.7 found before. We note that previous work by, e.g., Salim *et al.* (2007) also investigated the effect of statistical weighting on the sequence of star-forming galaxies. Their resulting best-fit slope for their UV-based SFRs is 0.65, between the two values reported here.

2.3. *AGN on the SFR-Stellar Mass Plane*

In this section, we examine the location of galaxies with AGN on the SFR-$M_\star$ plane relative to the full galaxy population. We split them in bins of AGN bolometric luminosity in order to assess whether their is a trend that we could interpret to learn about AGN fueling and/or feedback. We use both the V/V_{max} correction factors, and the obscured AGN fraction weights described previously in order to estimate the total AGN population. We do not distinguish between AGN types (Seyferts, Composites, LINERs; but see, e.g., Salim *et al.* 2007; Leslie *et al.* 2015). Figure 2 shows the resulting bivariate distributions for AGN separated in bins of bolometric luminosity. As we can see on the top row, the more luminous AGN ($L_{bol} > 45$) are preferentially located above or on the star forming sequence, while the lower luminosity bins occupy regions with decreasing SFR. At the low AGN luminosity end ($L_{bol} < 42$), AGN hosts are located below the star forming sequence, and overlapping with the population of passive galaxies.

However, we note that the lowest AGN luminosity bin includes an important number of LINERs, some of which may be so-called *retired* galaxies which can occupy the same regions of the BPT and VO87 as true LINERs even though their ionization emission is dominated by old stellar populations and/or shocks rather than AGN (e.g., Cid Fernandes *et al.* 2011; Yan & Blanton 2012). This would be consistent with LINER galaxies being predominantly colocated with passive galaxies. On the other hand, there are indications that a significant fraction of LINERs do host an AGN when following them up in different wave bands and/or stacking their X-ray emission (e.g., Ho 2008; Trouille *et al.* 2011; Trump *et al.* 2011, also see Section 3.2 by Juneau *et al.* 2011). Therefore, we consider the result of the lowest AGN luminosity to be ambiguous. An additional source of uncertainty at the low luminosity end comes from the difficulty of identifying weak AGN among strongly star-forming galaxies due to their lower fractional contribution to emission line fluxes, leading to a dilution of the AGN spectral signatures, and decreasing the completeness of AGN identification at low luminosities (Trump *et al.* 2015).

In contrast, the results at the high-luminosity end are much less subject to dilution of AGN emission line signatures. So we will focus our interpretation on these more reliable results. The fact that we find the most active AGN to reside in star-forming hosts supports a picture where the black hole fueling and star formation activity use a common gas reservoir and are both facilitated by the presence of a high gas content likely together with mechanisms that reduce the angular momentum of the gas. Conversely, while one would expect that the most luminous AGN would be the most capable of generating feedback that reduces or halts star formation in their hosts, their location on the SFR-$M_\star$ plane suggests that either they are not generating strong feedback, or that the effects from the feedback would be substantially delayed. It could also be the case that only in exceptional circumstances, such as major galaxy mergers, is strong AGN feedback playing an important role. This is supported by the scenario of two modes of quenching with a fast quenching in the case of major mergers aided with AGN feedback, while the bulk of galaxies would go through a slow quenching as they slowly use up their gas reservoir or as the latter gets hotter and no longer sustains star formation (e.g., Schawinski *et al.* 2014). However, these results are also consistent with cosmological simulations for which AGN feedback is a key ingredient to control both galaxy growh and black hole growth (e.g., Hirschmann *et al.* 2014)

Next, we divide the number of AGN hosts by the total number of galaxies in our sample over the SFR-$M_\star$ plane in order to calculate the AGN fraction (bottom row of Figure 2). From the left-hand side to right-hand side panels, we see an overall trend where the fraction of galaxies with luminous AGN is higher in hosts with elevated SFRs, which is qualitatively similar to the top row showing the bivariate distributions. However, an interesting distinction is that the AGN fraction is higher above and below the star-forming sequence than directly over it. This means that there is a larger spread of SFR values for AGN hosts at a given $M_\star$ compared to the bulk of the galaxy population. A physical origin of this difference would imply a process other than a strictly negative AGN feedback as the AGN hosts can be both over and under the sequence, or potentially it indicates the presence of more than one process at play.

If all galaxies in a given bin of SFR & $M_\star$ host a similarly massive black hole with episodes of accretion interspersed with episodes of inactivity, the fraction of AGN can be interpreted as a duty cycle (Novak *et al.* 2011; Gabor & Bournaud 2013; Schawinski *et al.* 2015). In the bottom row of Figure 2, the duty cycle would be defined as the fraction of the time that a given BH is accreting within the L_{bol} range of interest. As mentioned earlier, the two caveats at the low-luminosity end (nature of LINER-like emission, and incompleteness of AGN identification in star-forming hosts) prevent us from making a robust interpretation for that regime. The most interesting and also reliable trend is seen

in the $43 < log(L_{bol}) < 45$ bin (panel f), where we can see that galaxies with elevated SFR relative to the star-forming sequence are more likely to experience frequent AGN episodes. This result could be interpreted as a the presence of a gas reservoir facilitating both star formation and BH accretion.

2.4. *Implications & Lessons Learnt*

We found that the locus of AGN on the $SFR - M_\star$ plane varies as a function of AGN luminosity, itself a proxy of the black hole accretion rate. This means that there would not be a single answer to a question such as: *where are AGN located with respect to the star forming sequence?* Similarly, previous work reported a different level of SFR at a given $M_\star$ for AGN selected in different wavebands (e.g., radio, optical, IR; Ellison *et al.* 2016), and/or with different optical classification (LINER, composite, Seyferts; Leslie *et al.* 2015).

The division in terms of AGN luminosity can be used to infer information about AGN fueling and feedback. One would expect that higher luminosities imply both a more efficient fueling and the potential for more effective feedback (at least for radiation-driven feedback such as the *quasar* mode). Regarding the former, we found that AGN in the high luminosity bins live in hosts with elevated SFR, therefore supporting the idea of a common gas reservoir, and that the presence of this gas reservoir helps to sustain more frequent AGN episodes (from the fraction of galaxies with an AGN). In terms of feedback, the observed elevated SFRs in galaxies hosting luminous AGN instead suggest that the feedback is either unimportant or delayed. A limitation of this interpretation is that we do not know the past star formation history, and whether the SFRs were yet higher before the AGN was present or before it reached its current luminosity. For that reason, it is helpful to compare with cosmological simulations that include black hole growth and AGN feedback, such as the MAGNETICUM simulations with a revised AGN implementation (Hirschmann *et al.* 2014), as well as emission-line signature predictions (Hirschmann *et al.* 2017).

In addition, the relationship between AGN fueling, AGN feedback, and host galaxies properties may vary across cosmic time. Delvecchio *et al.* (2015) explored this topic by computing the average AGN accretion rate across the $SFR - M_\star$ plane between redshift $0 < z < 2.5$ for a sample of *Herschel* infrared-selected galaxies. The main conclusion from that work is that the accretion of the BH and the host growth track each other across cosmic time, and possibly more closely at $z > 0.8$ compared to low-redshift galaxies. While the sample size was limited (in particular in the lowest redshift bin), this work is a useful example to guide future statistical studies, though broadening to multiple selection techniques would be useful to understand variations with respect to other work. A complete picture requires an understanding of the AGN and host galaxy selection, and possibly splitting the samples into physically-motivated categories. Based on previous effort, the work presented here, and on discussion at the IAU Symposium, we list a few lessons:

• Correcting for the selection function arising from photometry and/or spectroscopy selection allows us to obtain more accurate representation of the relative galaxy (and AGN) subpopulations, for example using the V/V_{max} method;

• Performing multi-wavelength AGN analyses will remain key for sample completeness albeit it will require considering the various selection functions together;

• Relatedly, we might need to re-write the big questions to be more physically-specific rather than observationally-specific as we attempt to paint the global picture of AGN and galaxy co-evolution.
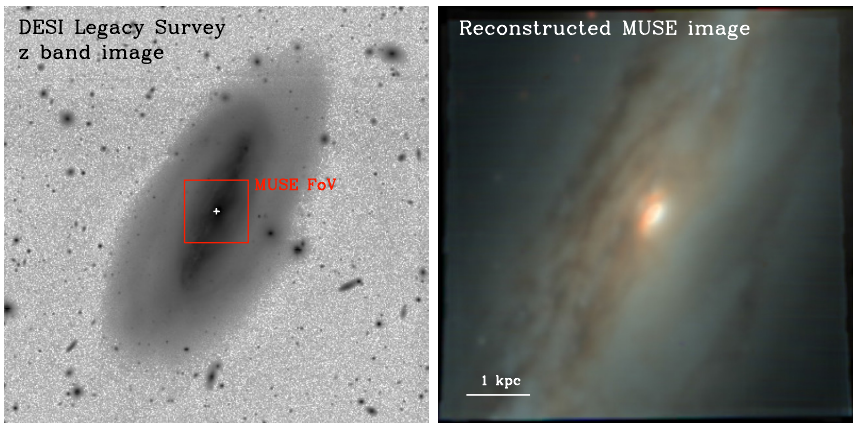
Figure 3. Images of galaxy NGC 7582. *(Left)* *z*-band image from the Dark Energy Spectroscopic Instrument (DESI) imaging Legacy Survey (Dey *et al.* 2019) to show the full extent of the galaxy. This image is 6.66' on a side, and we overlay the MUSE field-of-view with a $1' \times 1'$ square centered on the target. *(Right)* Color image constructed from the MUSE datacube by selecting 3 spectral windows for the red, green and blue channels that are free of emission lines as described by J19. We can see large-scale dust lanes as well as the highly reddened central region, which corresponds to a starburst surrounding the central AGN. North is up. East is to the left.

## 3. AGN fueling & feedback: A case study of NGC 7582

After considering a statistical study of AGN in nearby galaxies, we focus on a case study to investigate the relationship between AGN feedback and the host galaxy in a spatially resolved manner. Numerical simulations of isolated host galaxies with resolved ISM (reaching scales of a few pc) showed that the galaxy substructure can influence not only AGN fueling but also the impact of AGN feedback onto its surroundings (outflows and radiation; see, e.g., Gabor & Bournaud 2013 and Roos *et al.* 2015). Observational studies have also suggested a closer relationship between AGN fueling and the resolved, central SFR than with the total, galaxy-wide SFR (e.g., Diamond-Stanic & Rieke 2012).

We employed integral field spectroscopy to spatially resolve and map the ionized gas and stellar content of nearby AGN host NGC 7582, which is a barred spiral galaxy known to host both a central starburst and a heavily obscured AGN. Previous work with narrow-band imaging and integral field spectroscopy revealed the presence of extended narrow line regions (e.g., Morris *et al.* 1985; Riffel *et al.* 2009; Davies *et al.* 2016), which could in turn suggest a possible widespread influence of the AGN. The additional observations presented below augment previous effort with a combination of high spatial resolution (~ 1") over a 1 arcmin field-of-view spanning a scale of ~ 8 kpc at the distance to the target galaxy (Figure 3).

3.1. *Observations & Method*

NGC 7582 was observed with the Multi-Unit Spectroscopic Explorer (MUSE) instrument (Bacon *et al.* (2010)) on the Very Large Telescope (see Figure 3 for the MUSE field-of-view overlaid on the target galaxy). The observations, data reduction, spectral measurements, and inferred physical properties are described in detail elsewhere (Juneau *et al.*, in prep.; hereafter J19). In summary, the integration time on source was 40 minutes, with two short (1 minute) sky exposures offset from the target. The data were processed with the Reflex MUSE pipeline (Freudling *et al.* 2013, v1.0.5). The resulting datacube covers approximately a field-of-view of one square arcminute, with spaxels of
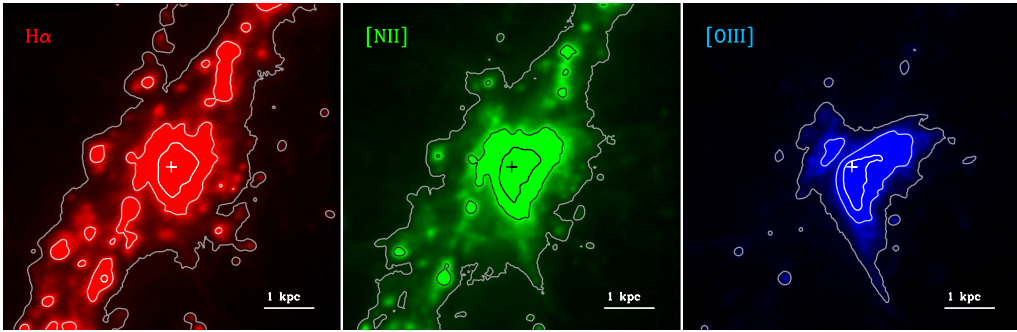
Figure 4. Intensity map for strong emission lines Hα (red), [N II] (green), and [O III] (blue). For each emission-line, we show the total line flux across the MUSE field-of-view. North is up; East is left. The scale bar corresponds to 1 kpc at the distance to NGC 7582. The plus symbol marks the center of the galaxy. Figure adapted from J19.

$0.2" \times 0.2"$ each. The spatial resolution is limited by the $\sim 1"$ seeing, and the spectral elements are 1.25 Å, which corresponds to $\sim 55 - 75\ km\ s^{-1}$ over the wavelength range of interest.

We fit the reduced datacube with the LZIFU package (Ho *et al.* 2016) in order to account for both the stellar continuum with spectral synthesis models (with pPXF; Cappellari & Emsellem 2004), and for the emission lines with Gaussian profiles. The fitting procedure was run in separate instances to fit the emission lines with one, and with two Gaussian components. We compared the results and assigned in post-processing the spaxels for which two components are needed to describe the observed [O III] $\lambda5007$ line profiles, which are the most likely tracers of the secondary ionized gas component associated with an outflow rather than with the systemic velocity. We identified such cases by applying a condition for the second component to be detected with a signal-to-noise ratio $S/N > 3$ in [O III].

3.2. *Maps of Ionized Gas*

The MUSE datacube includes several emission lines. In this section, we consider some of the commonly used strong lines, namely Hα, [N II] $\lambda6584$, and [O III] $\lambda5007$ (Figure 4). Hα traces well the total ionized gas, including gas ionized from young stars in H II regions, and other sources of ionization such as shocks and AGN photoionization. The Hα emission is distributed along the disk and bar of NGC 7582 spanning the entire MUSE field-of-view, as well as showing an important component from the central starburst and extending toward the AGN narrow line region. The clumpy or patchy appearance indicates the presence of star forming regions along the disk (and/or bar), and possible patchy obscuration although the Hα-bright regions also tend to exhibit elevated dust obscuration according to the Hα/Hβ Balmer Decrement. As described by J19, we converted the Balmer Decrement to gas attenuation by assuming an intrinsic ratio $(Hα/Hβ)_0 = 2.86$ ($n_e = 100$ cm^{-3}; $T_e = 10^4$ K; Osterbrock & Ferland 2006), and the Calzetti extinction law (Calzetti *et al.* 2000).

On the middle panel of Figure 4, we can see that the [N II] emission is largely co-located with Hα except that it is comparatively less prominent along the disk and bar, and more prominent on the central starburst and AGN ionization cone region. For H II regions, the [N II]/Hα ratio is commonly used as an indicator of the gas-phase metallicity. For AGN narrow-line regions, the ratio can be further enhanced due to a combination of high metallicity and harder ionizing spectrum (e.g., Kewley *et al.* (2013)). The [O III] emission (right-hand panel of Figure 4) is largely concentrated on the AGN ionization cones. In this
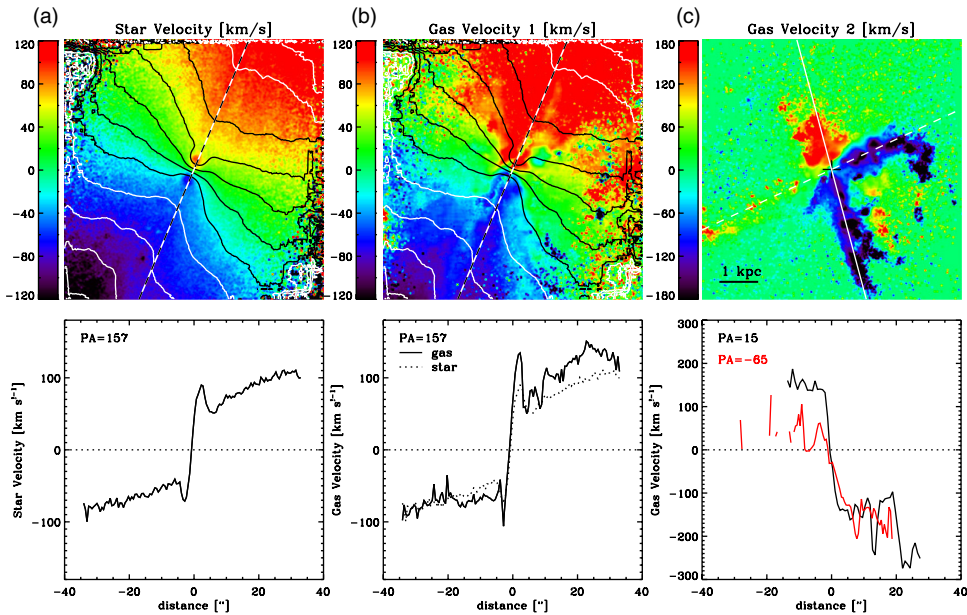
Figure 5. Top row: velocity maps with iso-contours of the stellar velocity field. The PA of 157 is shown with the dashed line. (a) Stellar velocity map (in km s^{-1}); (b) Gas velocity map (in km s^{-1}) for Component 1; (c) Gas velocity map (in km s^{-1}) for Component 2. North is up; East is left. The scale bar corresponds to 1 kpc at the distance of the target. Bottom row: velocity profile (in km s^{-1}) along PA = 157 for the stellar and gas components. (d) Stellar velocity profile, which shows a clear velocity excess at the KDC while the main curve is slowly rising in amplitude with distance away from the center. (e) Nebular gas velocity profile for Component 1 (solid line) compared to the stellar profile from panel d (dotted line). (f) Nebular gas velocity profile for Component 2 along axes defined to follow the edges of the cones with PA = 15 (black line; solid line in panel c), and PA = −65 (red line; dashed line in panel c). Figure adapted from J19.

case, one can see both the front cone and back cone (i.e., counter-cone) which is behind the host galaxy from our line-of-sight. The dearth of [O III] emission along the star forming knots is consistent with metal-rich gas.

In the full analysis by J19, the combination of those three strong emission lines with the addition of Hβ and [S II] $\lambda\lambda 6717, 6731$ are used to produce line ratio maps in order to apply the BPT and VO87 diagnostic diagrams. The results indicate that the star forming disk and bar are consistent with metal-enriched star forming dominated regions surrounded by diffuse medium (possibly warm-hot interstellar medium, or WHIM). The cones were found to have Seyfert-like line ratios indicating AGN photoionization. The areas on either side of the cones are characterized by LINER-like ratios, which could potentially indicate shock-excitation. This possible interpretation is consistent with the outflowing kinematics of the cones, which we describe in the next section.

3.3. *Star & Ionized Gas Kinematics*

The star and gas kinematics, respectively derived from the continuum fitting, and emission line fitting with LZIFU, are shown in the top row of Figure 5. The velocity maps show a clear large-scale rotation of the host galaxy for both the stellar component (panel a) and the first gas component (panel b). By definition, the second gas component was attributed to spaxels which had a significant second (or offset) component in the [O III] $\lambda 5007$ emission line. It clearly shows a biconical outflows originating from the

center of the galaxy, with a blue-shifted front cone and a redshifted back cone. The projected velocities of the outflowing ionized gas reach around ± 200 km s^{-1}. While the first gas component is characterized by motion more similar to the stellar component, there are also some notable differences. For instance, the velocity field is generally less regular, suggesting motion beyond a pure simple rotating disk. In particular, there appear to be mild deviations parallel to the PA, which is also the angle of the bar, and which could suggest gas streaming along the leading edge of the bar.

The bottom row displays the velocity profiles along the galaxy PA (157 degrees East of North) for the stellar and first gas component, and the velocity profiles along the edges of the cones for the second gas component (angles of 15 and -65 degrees, as shown in panel c). The velocity profiles for the stellar component clearly shows enhanced features near the center corresponding to a kinematically distinct core (KDC) with respect to the larger scale rotation. The KDC is rotating in the same direction as the galactic disk but with a differential, elevated velocity (by approximately 40 km s^{-1}). The KDC shows as two spots on the velocity field from panel a, and likely corresponds to a disk or ring of material. As described in J19, a ring interpretation is favored due to the likely spatial coincidence with the inner Lindblad resonance of the bar, and furthermore the presence of the AGN and associated outflows, which are possibly driving material away from the inner portion of the ring. The velocity profile for the first gas component is similar to that of the stars except for presenting a systematic offset along the redshifted side by about 40 km s^{-1}. It is possible that this difference arises due to the known presence of a large-scale bar in this galaxy that could affect the motion of the gas along the PA traced in panel b. Lastly, the velocity profiles along the edges of the biconical outflows suggest comparable velocities between the front and back cones along PA $= 15$, where we can see both components. We lack the bulk of the redshifted component along PA $= -65$, possibly due to the presence of foreground dust lanes in the host galaxy obscuring the optical light emission.

3.4. *Implications & Lessons Learnt*

Putting together the results on the gas ionization, gas kinematics, and stellar kinematics for the central ~ 8 kpc of NGC 7582, we paint an overall picture where nuclear ionized gas outflows have a symmetrical and biconical shape, and are predominantly AGN-photoionized. Their opening angle and the spatial coincidence of the base of the cones with the central KDC suggest that the latter may be responsible for collimating them. We thus propose that the outflows are AGN-driven but (re-)collimated by the host galaxy substructure, similarly to what Prieto *et al.* (2014) previously postulated (also see Ricci *et al.* 2018). If that were the case, then the host galaxy substructure would play a role in how the feedback from the central AGN affects the host galaxy. Here, the central KDC may be protecting or shielding the host galaxy material from the effects of AGN outflows. More work is needed to assess how common this scenario may be among AGN hosts. Overall, this interpretation implies that we may need to revisit the interplay between the central AGN and the host galaxy substructure in order to fully understand the connection between supermassive black holes and galaxies. We also conclude that integral field spectroscopy − also known as 3D spectroscopy − is a useful tool to investigate this question (see also, e.g., Husemann *et al.* 2019).

References

Abazajian, K. N., Adelman-McCarthy, J. K., Agüeros, M. A., *et al.* 2009, *ApJS*, 182, 543
Alexander, D. M. & Hickox, R. C. 2012, *NewAR*, 56, 93
Bacon, R., Accardo, M., Adjali, L., *et al.* 2010, *SPIE Conference Series*, Vol. 7735, id. 773508

Baldwin, J. A., Phillips, M. M., & Terlevich, R. 1981, *PASP*, 93, 5

Bassani, L., Dadina, M., Maiolino, R., *et al.* 1999, *ApJS*, 121, 473

Beckmann, R. S., Devriendt, J., Slyz, A., Peirani, S., *et al.* 2017, *MNRAS*, 472, 949

Bongiorno, A., Merloni, A., Brusa, M., Magnelli, B., *et al.* 2012, *MNRAS*, 427, 3103

Bower, R. G., Benson, A. J., Malbon, R., Helly, J. C., *et al.* 2006, *MNRAS*, 370, 645

Brinchmann, J., Charlot, S., White, S. D. M., *et al.* 2004, *MNRAS*, 351, 1151

Calzetti, D., Armus, L., Bohlin, R. C., *et al.* 2000, *ApJ*, 533, 682

Cappellari, M. & Emsellem, E., 2004 *PASP*, 116, 138

Chen, C.-T. J., Hickox, R. C., Alberts, S., Brodwin, M., *et al.* 2013, *ApJ*, 773, 3

Cid Fernandes, R., Stasínska, G., Mateus, A., & Vale Asari, N. 2011, *MNRAS*, 413, 1687

Ciotti, L., Ostriker, J. P., & Proga, D. 2010, *ApJ*, 717, 708

Cisternas, M., Jahnke, K., Inskip, K. J., *et al.* 2011, *ApJ*, 726, 57

Croton, D. J., Springel, V., White, S. D. M., *et al.* 2006, *MNRAS*, 365, 11

Davies, R. L., Groves, B., Kewley, L. J., *et al.* 2016, *MNRAS*, 462, 1616

Delvecchio, I., Lutz, D., Berta, S., Rosario, D. J., *et al.* 2015, *MNRAS*, 449, 373

Dey, A., Schlegel, D. J., Lang, D., Blum, R., *et al.* 2019, *AJ*, 157, 168

Diamond-Stanic, A. M. & Rieke, G. H. 2012, *ApJ*, 746, 168

Ellison, S. L., Teimoorinia, H., Rosario, D. J., & Mendel, T. 2016, *MNRAS*, 458, L34

Fabian, A. C. 2012, *ARA&A*, 50, 455

Ferrarese, L. & Merritt, D. 2000, *ApJ*, 539, L9

Freudling, W., Romaniello, M., Bramich, D. M., *et al.* 2013, *A&A*, 559, A96

Gabor, J. M. & Bournaud, F. 2013, *MNRAS*, 434, 606

Gabor, J. M. & Davé, R. 2012, *MNRAS*, 427, 1816

Gavazzi, *et al.* 2015, *A&A*, 580, 13

Grogin N. A., Conselice, C. J., Chatzichristou, E., Alexander, D. M., *et al.* 2005, *ApJ*, 627, L97

Groves, B., Brinchmann, J., & Walcher, C. J. 2012, *MNRAS*, 419, 1402

Harrison, C. M., Costa, T., Tadhunter, C. N., Flütsch, A., *et al.* 2018, *NatAs*, 2, 198

Harrison, C. M. 2017, *NatAs*, 1, 16

Hickox, R. C., Jones, C., Forman, W. R., *et al.* 2009, *ApJ*, 696, 891

Hirschmann, M., Charlot, S., Feltre, A., *et al.* 2017, *MNRAS*, 472, 2468

Hirschmann, M., Dolag, K., Saro, A., *et al.* 2014, *MNRAS*, 442, 2304

Ho, I.-T., Medling, A. M., Groves, B., *et al.* 2016, *Ap&SS*, 361, 280

Ho, L. C. 2008, *ARA&A*, 46, 475

Husemann, B., Scharwächter, J., Davis, T. A., *et al.* 2019, *arXiv e-prints*, arXiv:1905.10385

Jahnke, K. & Maccío, A. V. 2011, *ApJ*, 734, 92

Juneau, S., Bournaud, F., Charlot, S., *et al.* 2014, *ApJ*, 788, 88

Juneau, S., Dickinson, M., Bournaud, F., Alexander, D. M., *et al.* 2013, *ApJ*, 764, 176

Juneau, S., Dickinson, M., Alexander, D. M., & Salim, S. 2011, *ApJ*, 736, 104

Karouzos, M., Im, M., Trichas, M., Goto, T., *et al.* 2014, *ApJ*, 784, 137

Kartaltepe, J. S., Sanders, D. B., Le Floc'h, E., Frayer, D. T., *et al.* 2010, *ApJ*, 721, 98

Kauffmann, G., Heckman, T. M., White, S. D. M., *et al.* 2003a, *MNRAS*, 341, 33.

Kauffmann, G., Heckman, T. M., Tremonti, C., *et al.* 2003b, *MNRAS*, 346, 1055

Kewley, L. J., Dopita, M. A., Leitherer, C., *et al.* 2013, *ApJ*, 774, 100

Kewley, L. J., Groves, B., Kauffmann, G., & Heckman, T. 2006, *MNRAS*, 372, 961

Kewley, L. J., Dopita, M. A., Sutherland, R. S., *et al.* 2001, *ApJ*, 556, 121

Lamastra, A., Bianchi, S., Matt, G. *et al.* 2009, *A&A*, 504, 73

Leslie S. K., Kewley L. J., Sanders, D. B., & Lee, N. 2015 *MNRAS*, 455, 82

Lusso, *et al.* 2013, *ApJ*, 777, 28

Magorrian J. *et al.* 1998, *AJ*, 115, 2285

Morris, S., Ward, M., Whittle, M., Wilson, A. S., & Taylor, K. 1985, *MNRAS*, 216, 193

Mullaney, J. R., Alexander, D. M., Aird, J., Bernhard, E., *et al.* 2015, *MNRAS*, 453, 83

Novak G. S., Ostriker J. P., & Ciotti L. 2011, *ApJ*, 737, 26

Osterbrock, D. E. & Ferland, G. J. 2006, *U*niversity Science Books, Astrophysics of Gaseous Nebulae and Active Galactic Nuclei, 2edn.

Prieto, M. A., Mezcua, M., Fernández-Ontiveros, J. A., & Schartmann, M. 2014, *MNRAS*, 442, 2145

Ricci, T. V., Steiner, J. E., May, D., Garcia-Rissmann, A., & Menezes, R. B. 2018, *MNRAS*, 473, 5334

Riffel, R. A., Storchi-Bergmann, T., Dors, O. L., & Winge, C. 2009, *MNRAS*, 393, 783

Roos, O., Juneau, S., Bournaud, F., & Gabor, J. M. 2015, *ApJ*, 800, 19

Rosario, D. J., Santini, P., Lutz, D., Netzer, H., *et al.* 2013, *ApJ*, 771, 63

Salim, *et al. ApJS*, 173, 267

Schawinski, K., Koss, M., Berney, S., & Sartori, L. F. 2015, *MNRAS*, 451, 2517

Schawinski, K., Urry, C. M., Simmons, B. D., *et al.* 2014, *MNRAS*, 440, 889

Schawinski, K., Thomas, D., Sarzi, M., *et al.* 2007, *MNRAS*, 382, 1415

Schaye, J., Crain, R. A., Bower, R. G.; Furlong, M., *et al.* 2015, *MNRAS*, 446, 521

Silverman, J. D., Lamareille, F., Maier, C., Lilly, S. J., *et al.* 2009, *ApJ*, 696, 396

Simpson, C. 2005, *MNRAS*, 360, 565

Steinborn, L. K., Hirschmann, M., Dolag, K., Shankar, F., *et al.* 2018, *MNRAS*, 481, 341

Tanaka, M. 2012, *PASJ*, 64, 37

Treister, E., Schawinski, K., Urry, C. M., & Simmons, B. D. 2012, *ApJ*, 758, 39

Tremonti, C. A., Heckman, T. M., Kauffmann, G., *et al.* 2004, *ApJ*, 613, 898

Trouille, L., Barger, A. J., & Tremonti, C. 2011, *ApJ*, 742, 46

Trump, J. R., Weiner, B. J., Scarlata, C., *et al.* 2011, *ApJ*, 743, 144

Trump, J. R., Sun, M., Zeimann, J. R., *et al.* 2015, *ApJ*, 811, 26

Veilleux, S. & Osterbrock, D. E. 1987, *ApJS*, 63, 295

Yan, R. & Blanton, M. R. 2012, *ApJ*, 747, 61